Comprehensive Study on Cell Components in High-Voltage Pouch Cells with Lithium Perchlorate: Decomposition, Transesterification, Chlorination, Deposition, and Self-Discharge

Matthias Weiling,[a] Felix Pfeiffer,[a] Christian Lechtenfeld,[b] Silvan Stuckenberg,[b] Nick Fehlings,[b] Lars Frankenstein,[b] Verena Küpers,[b] Jian-Fen Wang,[a] Sascha Nowak,[b] and Masoud Baghernejad*[a]

Battery development has traditionally focused on high energy and long lifetime cells, but there is now a shift towards their sustainability and safety. One example of this trend is the search for fluorine-free conductive salts. The overwhelming majority of lithium-ion conductive salts contain fluorine, which is critical regarding their environmental impact, sustainability, and toxicology. In this study, we perform a comprehensive investigation of the performance and aging mechanisms of cell components with $LiClO_4$ as conductive salt in high-voltage NMC622∥Graphite pouch cells. The cells containing $LiClO_4$ show poorer electrochemical performance compared to their $LiPF_6$ equivalents. However, to the best of our knowledge, a mechanistic understanding of the effect of $LiClO_4$ on the aging of electrode and electrolyte components for high-voltage cells is largely missing. Developing such an understanding will pave the way toward designing alternative salts to $LiPF_6$, ultimately leading to fluorine-free and more sustainable battery cells. Our results show, that the chlorination of ethyl methyl carbonate at both methyl and ethyl groups and the formation of large $(Li_w)Al_xO_yCl_z$ composite deposits on the cathode surface result from perchlorate degradation at the cathode. This leads to increased cell resistance, reduced capacity retention, and accelerated degradation of the $LiClO_4$-containing electrolytes.

1. Introduction

The commitment to the electrification of the transportation sector is a major driving force in accelerating and increasing lithium-ion battery (LIB) mass production.[1–3] While further growth of the LIB market is imminent, increasing the energy density of LIB cells to 500 Wh kg^{-1} and beyond may be one of the greatest challenges of this decade.[4–6] In this attempt, it is also inevitable to focus on enhancing the sustainability of the usually environmentally- and toxicologically-critical LIBs.

Different approaches to increase the energy density of LIB cells are being extensively researched. Increasing the mass loadings of the anode and cathode might be one of the most straightforward steps to achieve higher energy densities.[7,8]

However, this typically reduces the electrochemical performance and power density as higher mass loadings impede ion diffusivity and electronic conductivity.[9] Another simple step to increase the LIB energy density while retaining power density is widening the operational voltage window.[8,10–12] However, exceeding the electrochemical stability limits of the electrodes and electrolyte leads to accelerated degradations by undesired irreversible reactions.[10,12] For example, "rollover" failure, which is sudden rapid capacity fading as a result of lithium plating on the anode induced by transition metal (TM) crosstalk, is a well-known issue.[8,13–15]

Degradation of the conductive salt $LiPF_6$ in state-of-the-art non-aqueous carbonate-based electrolytes is critical due to the formation of highly toxic fluorinated products.[16,17] Most of these evolving fluorinated are already investigated and understood to a large extent. For instance, HF is known to facilitate TM dissolution, while (organo−)fluorophosphates, such as difluorophosphate (LiDFP), were found to increase the lifetime and electrochemical performance of high-voltage LIB cells. These compounds scavenge TMs in the bulk electrolyte, mitigating the rollover failure.[8,13,18,19] Further widely used fluorinated compounds in batteries are the common binder material polyvinylidene fluoride (PVDF) or the state-of-the-art additive fluoroethylene carbonate (FEC), which belong to the environmentally and toxicologically critical per- and polyfluoroalkyl substances (PFAS) family. Albeit lithium and fluorine are "ideal partners", eliminating fluorine from LIBs is necessary to produce "greener" batteries.[20,21]

[a] M. Weiling, F. Pfeiffer, J.-F. Wang, M. Baghernejad
Helmholtz-Institute Münster, IMD-4, Forschungszentrum Jülich GmbH, Corrensstrasse 46, 48149 Münster, Germany
E-mail: b.masoud@fz-juelich.de

[b] C. Lechtenfeld, S. Stuckenberg, N. Fehlings, L. Frankenstein, V. Küpers, S. Nowak
MEET Battery Research Center Münster, University of Münster, Corrensstrasse 46, 48149 Münster, Germany

Most of the alternative salts to $LiPF_6$, such as $LiAsF_6$, $LiBF_4$, LiDFOB (Li difluoro(oxalato)borate), or LiTFSI (bis(trifluoromethanesulfonyl)imide) and its derivatives, are highly fluorinated.[22–24] As an exception, LiBOB (Li bis(oxalate)borate) is fluorine-free, however, its low solubility, poor ionic conductivity, and narrow electrochemical stability window result in low electrochemical performance in high-voltage LIBs.[25–27]

In this study, lithium perchlorate ($LiClO_4$), a fluorine-free alternative to $LiPF_6$, is revisited for its potential application in high-voltage LIB cells. $LiClO_4$ has already been used as a conductive salt in the early batteries due to high ionic conductivity, good thermal and electrochemical reductive stability, low moisture sensitivity, and suitable aluminum current collector passivation.[16,28–33] Furthermore, $LiClO_4$ is relatively inexpensive and easy to purify.[29] Especially, the lack of HF formation, either due to the absence of fluorine or a low moisture sensitivity, in electrolytes was found to increase the charge/discharge cycling stability by preventing transition metal dissolution from the cathode, such as Fe from lithium iron phosphate cathodes.[34,35] Additionally, the lack of fluorine in $LiClO_4$ also prevents the formation of the above-mentioned environmentally and toxicologically critical fluorinated substances. However, perchlorate is highly oxidizing and may react with organic solvents in LIBs under extreme conditions, even resulting in detonated cells in abuse investigations with lithium metal, as shown by Newman et al.[16,28,36] Nevertheless, under high-voltage conditions perchlorate may undergo increased degradation in the cell, which may lead to increased perchlorate-mediated interphase formation and electrolyte aging. Similar to LiDFP, these degradation products might exhibit beneficial effects. Understanding the degradation mechanisms and products of the already used conductive salts is necessary for a knowledge-based design of alternative salts for future high-performance electrolyte formulations.

As expected, the galvanostatic charge/discharge cycling experiments of high-voltage NMC622||artificial graphite (AG) cells in the presence of 1.0 M $LiClO_4$ in EC/EMC (3:7, by weight) show inferior performance compared to the $LiPF_6$ equivalent. Even the addition of FEC as a fluorine-containing film-forming additive to the $LiClO_4$ electrolyte did not lead to a major improvement in the electrochemical performance. Thus, not only the missing fluorine in the electrolyte but also additional mechanisms caused by $LiClO_4$ influence the performance of the cells. To the best of our knowledge, the underlying mechanism of the working principle and degradation products of $LiClO_4$, which result in lower electrochemical performance compared to $LiPF_6$-based cells, has not been systematically investigated in LIB cells, especially at high voltage.

Towards this end, attenuated total reflection Fourier-Transform infrared (ATR-FTIR) spectroscopy and gas chromatography-mass spectrometry (GC-MS) investigations of the electrochemically aged electrolytes identified not only transesterification but also chlorination of EMC. This occurs as a result of perchlorate reduction to chlorate and chloride, observed with ion chromatography-conductivity detection-mass spectrometry, which are presumably forming chlorine radicals. Eventually, hydrogen abstraction and chlorine addition lead to three different chlorinated EMC species at the ethyl and methyl positions. Further surface morphology investigations on the cathode via scanning electron microscopy (SEM) of the aged electrodes revealed deposits with a size of up to 100 μm, which were identified with energy dispersive X-ray (EDX) and Raman spectroscopy to be a $(Li_w)Al_xO_yCl_z$ composite.

2. Results and Discussion

2.1. Electrochemical Investigations

The specific discharge capacities of NMC622||AG pouch cells with $LiPF_6$, $LiClO_4$, and $LiClO_4+FEC$ electrolytes are shown in Figure 1a. Ongoing charge/discharge cycling exhibits faster capacity fading rates for cells with $LiClO_4$ than for cells with $LiClO_4+FEC$ and $LiPF_6$. The cells reach 80% state of health (SoH) after 120 cycles with $LiPF_6$, 63 cycles with $LiClO_4+FEC$, and 45 cycles with $LiClO_4$. The full figure (up to 350 cycles) and a comparison with cells containing LiBOB, $LiBF_4$, and LiTFSI can be found in Figure S1 and S2 in the Supporting Information. Note, that cells containing the other fluorine-free alternative LiBOB exhibit lower electrochemical performance than the cells with $LiClO_4$.

The differences in capacity fading rates are mostly related to interphase formation and internal resistance, which are detrimental to the electrochemical performance if insufficient and high, respectively. Furthermore, insufficient interphase formation gives rise to ongoing irreversible reactions, accelerating the rate of active lithium loss and electrolyte consumption, resulting in faster cell components aging. The interphase formation and irreversible side reactions are evaluated by analysis of the corresponding charge and discharge capacities and Coulombic efficiencies (CEs) in the following paragraphs.

As the interphases are initially formed by irreversible reactions in the formation cycles, the quantity of these reactions is indicated by the initial capacities and CEs.[37,38] Note that the CEs in the formation cycles do not necessarily correspond to the effectivity of the formed interphases. For example, additional irreversible reactions in the formation cycles might stem from film-forming additives to form an effective interphase, whereas ongoing electrolyte degradation results in non-effective interphases.

The discharge capacities of the first formation cycles are 158 ± 1 mAh g^{-1} for cells with $LiPF_6$, 155 ± 1 mAh g^{-1} with $LiClO_4+FEC$, and 151 ± 1 mAh g^{-1} with $LiClO_4$. As shown in Figure 1b, the highest initial Coulombic efficiency (ICE), indicating the ratio of irreversible to reversible reactions in the first formation cycle, is obtained for the cells with $LiClO_4+FEC$ ($87.6\pm0.1\%$), followed by cells with $LiPF_6$ ($87.0\pm0.2\%$), and cells with just $LiClO_4$ ($86.3\pm0.8\%$). This results in a total of 23 ± 1 mAh g^{-1} irreversible reactions during charge for cells with $LiPF_6$, 22 ± 1 mAh g^{-1} with $LiClO_4+FEC$, and 24 ± 2 mAh g^{-1} with $LiClO_4$. Comparing $LiClO_4$ with $LiClO_4+FEC$, FEC is reduced additionally, but overall this leads to less irreversible reactions in the cell.
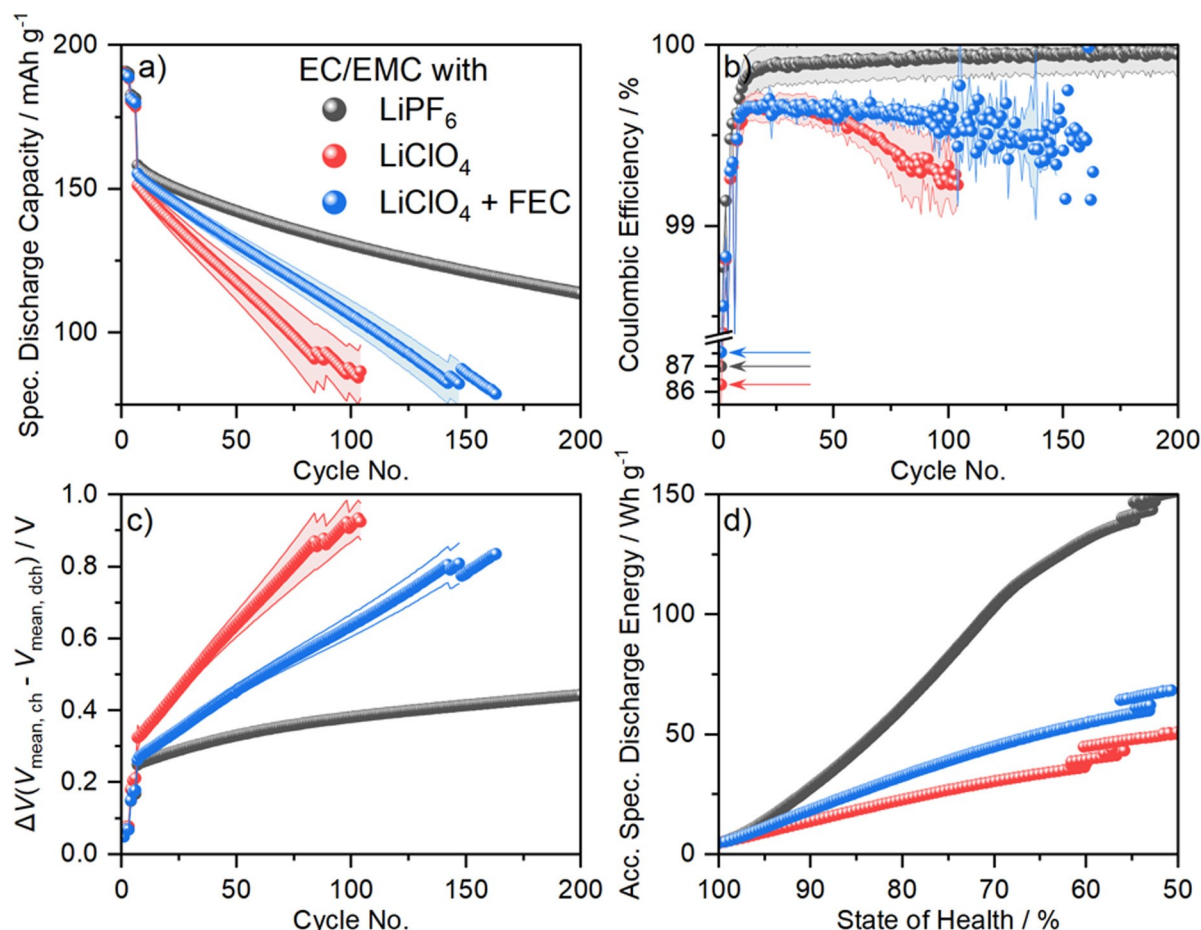
Figure 1. a) Specific discharge capacities at 1 C charge/discharge, b) Coulombic efficiencies, c) voltage difference of the mean charge and mean discharge voltage per half-cycle, and d) accumulated specific discharge energy of NMC622||AG pouch cells with 1.0 M LiPF$_6$, 1.0 M LiClO$_4$, and 1.0 M LiClO$_4$ with 0.1 M FEC in EC/EMC (3:7, by weight) at 20 °C in a voltage operational window 4.5–2.8 V. The state of health was calculated using the capacity of the 7th cycle of a cell as a reference (first cycle after formation).

This indicates better surface passivation in the cells with LiClO$_4$ + FEC compared to LiClO$_4$.

The electrochemical stability of the formed interphases can be indicated by the CEs in the following cycles. In the following formation cycles, the CEs of cells with LiClO$_4$ and LiClO$_4$ + FEC are lower than the CEs of cells with LiPF$_6$, indicating a higher quantity of interfacial irreversible reactions during cell cycling. The lower CEs in the formation cycles of cells with LiClO$_4$ and LiClO$_4$ + FEC compared to LiFP$_6$ indicate an insufficient electrode passivation and thus insufficient interphase formation. With ongoing charge/discharge cycling, the cells with LiPF$_6$ exhibit a slightly increasing CE from 99.9 ± 0.1 % (cycle 20) to 100.0 ± 0.1 % (cycle 200), whereas the cells with LiClO$_4$ + FEC exhibit a somewhat decreasing CE 99.66 ± 0.02 % (cycle 20) to 99.61 ± 0.05 % (cycle 90). The CEs of cells with LiClO$_4$ are decreasing at a faster rate, from 99.64 ± 0.07 % (cycle 20) to 99.4 ± 0.2 % (cycle 90), indicating a faster irreversible loss of active lithium.

Besides irreversible reaction rates in defining the active lithium loss in the cells, increased cell resistance may also contribute to capacity loss. ΔV analysis, obtained by subtracting the mean discharge from the mean charge voltage, can be used to estimate the internal resistance of the cells at each charge/discharge cycle (Figure 1c).[11,37,39,40] The trends of the ΔV values in Figure 1c are inversely mirroring the slope of the specific discharge capacities (Figure 1a), indicating a strong correlation. The ΔV values of cells with LiClO$_4$ after formation (330 ± 30 mV) are higher compared to cells with LiPF$_6$ (250 ± 10 mV) or LiClO$_4$ + FEC (260 ± 10 mV). An intrinsic reason for the overall higher internal resistance of the cells containing LiClO$_4$ in the first few cycles might be the lower ionic conductivity of the LiClO$_4$-containing electrolyte (5.18 mS cm^{-1} at 20 °C) compared to the LiPF$_6$-containing electrolyte (8.04 mS cm^{-1} at 20 °C), as shown in Figure S4 in the Supporting Information. The higher internal cell resistance in the cells containing LiClO$_4$ is assumed to be a cause for the lower initial discharge capacities of the cell at 1 C, as the cut-off voltages at 4.5 V and 2.8 V are reached faster. With ongoing charge/discharge cycling, the ΔV is increasing on average about 7 mV per cycle in the case of cells with LiClO$_4$, 4 mV per cycle with LiClO$_4$ + FEC, and 1 mV per cycle with LiPF$_6$. Thus, it is assumed that the faster degradation of the electrodes and the electrolyte with LiClO$_4$ is responsible for a higher rate of internal resistance increase. This can be linked to a higher

Batteries & Supercaps

Research Article
doi.org/10.1002/batt.202400568

Chemistry Europe
European Chemical
Societies Publishing

rate of irreversible reactions in the case of cells with LiClO$_4$, which is indicated by the lower CEs, as discussed above.

The accumulated specific discharge energy density *vs.* SoH, shown in Figure 1d, allows a fair comparison of the overall electrochemical performance of the cells with the different electrolyte formulations. By this, the relative contribution of all effects, like differences in discharge capacities, internal resistance, failure mechanisms, and capacity fading, are captured.[10] Overall, the addition of FEC to cells with LiClO$_4$ leads to a higher accumulated specific discharge energy until 80% SoH of about 33 ± 1 Wh g^{-1} compared to 23 ± 1 Wh g^{-1} without FEC. In the case of LiPF$_6$, an accumulated energy of 62 ± 1 Wh g^{-1} is drawn from the cells until 80% SoH.

Generally, the electrochemical performance of high-voltage NMC622||AG cells with LiClO$_4$ as conductive salt is inferior compared to the LiPF$_6$ equivalent. By the addition of FEC to the LiClO$_4$ electrolyte, the influence of fluorine is showcased. However, by adding FEC as a film-forming additive, the electrochemical performance of the cells could not be improved to achieve a similar performance as with LiPF$_6$.

2.2. Electrolyte Investigation

To identify and understand the underlying degradation mechanisms and products in the cells containing LiClO$_4$, the electrochemically aged electrolytes and electrodes have to be investigated. Employing ATR-FTIR spectroscopy, GC-MS, IC–CD-MS, and total reflection X-Ray fluorescence (TXRF) spectroscopy, the extracted electrolytes from the electrochemically aged cells are probed complementary. By this, the elemental, molecular, and ionic species in the electrolyte are identified toward understanding the associated degradation mechanisms of the corresponding cells.

In this regard, the electrochemically aged electrolytes were extracted from the respective cells at 50% SoH and compared with the pristine electrolytes by ATR-FTIR spectroscopy. The obtained spectra in the region of 960–750 cm^{-1} (Figure 2) and the highlighted bands around 853 and 914 cm^{-1} are discussed below. Compared to the full spectra in the region from 1900-550 cm^{-1} (Figure S5) of the pristine electrolyte, only these two highlighted bands are observed to evolve or change notably.

In the spectra of the aged LiClO$_4$ and LiClO$_4$+FEC electrolytes in Figure 2, an additional band around 853 cm^{-1} can be observed, which is not visible in the pristine electrolytes. A higher intensity in the case of the aged LiClO$_4$ electrolyte is observed compared to the LiClO$_4$+FEC electrolyte. Thus, it can be assumed that FEC plays a role in suppressing the evolution of the species corresponding to the band around 853 cm^{-1}. The comparison of the pristine and electrochemically aged electrolytes with LiPF$_6$ as conductive salt does not allow a clear statement about the band around 853 cm^{-1}, as this region is superimposed by the absorption of ν(P–F) by the PF$_6$ anion.[37] Additionally, a small absorbance increase is found around 914 cm^{-1} in the electrochemically aged LiClO$_4$ and LiPF$_6$ electrolytes, compared to the respective pristine electrolytes. A comparison of the spectra in Figure 2 with the reference spectra
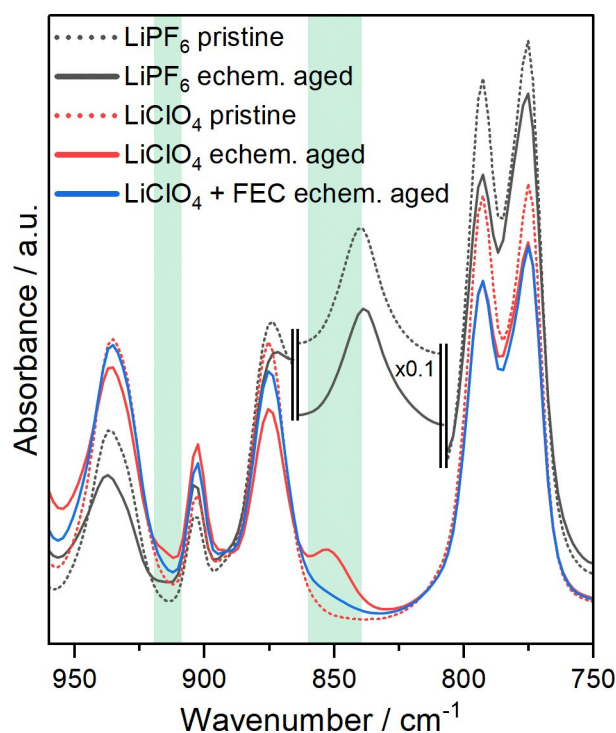

Figure 2. ATR-FTIR spectra from pristine and electrochemically aged EC/EMC (3:7, by weight) electrolytes with LiPF$_6$, LiClO$_4$, and LiClO$_4$+FEC electrolyte. The pristine electrolytes were mixed with 1.0 M LiPF$_6$ or LiClO$_4$; 0.1 M FEC was used for the pristine FEC-containing electrolyte. The electrochemically aged electrolytes were extracted from NMC622||AG cells charge/discharge cycled between 4.5–2.8 V to 50% SoH. The full spectra are given in Figure S5. For better visibility, the band around 838 cm^{-1} in the spectra of the LiPF$_6$-containing electrolytes was reduced by a factor of 10 in the region from 864–808 cm^{-1}.

of possible degradation products of the electrolyte, current collector, or pouch cell electrode tape in Figure S6 leads to the conclusion, that the band around 853 cm^{-1} can be assigned to DEC and the band around 914 cm^{-1} can be assigned to dimethyl carbonate (DMC).[41] In previous studies, the underlying vibration modes $\delta_{rocking}(CO_2)+\nu_{asym}(O-C-C)$,[42] $\delta_{rocking}(CH_2)$,[43] or $\nu(C-C)+\nu(C_{ether}-O)$[44] are suggested for the band around 853 cm^{-1} of DEC. However, DFT calculations performed in this study suggest $\delta_{scissoring}(CO_2)+\nu(C_{ether}-O)+\delta_{asym.\,bend.}(CH_3)$, as shown in Figure S7. The underlying vibration mode of the band at 914 cm^{-1} can be assigned to $\nu(CH_3-O)$ of DMC.[45]

DMC and DEC are well-known products from the transesterification of EMC.[38,46–51] The transesterification mechanism is known to be caused by insufficient electrode passivation, which can be overcome by *e.g.* implementation of film-forming additives, such as vinylene carbonate or FEC.[38,47–51] Furthermore, transesterification is an ongoing process, which leads to the accumulation of DMC and DEC in the electrolyte during charge/discharge cycling. Vice versa, the amounts of DMC and DEC in different electrolytes can indicate cell aging. However, distinguishing between calendar and electrochemical aging in spent LIBs is not reasonable, as both aging processes show different rates.

The presence of DMC and DEC in the electrochemically aged electrolytes is further investigated by GC-MS. To increase

the effect of electrochemical aging of the LiClO$_4$-containing electrolyte, additional cells with LiClO$_4$ were also charge/discharge cycled to 25% SoH. The total ion chromatogram (TIC) of the aged electrolyte with LiClO$_4$ cycled to 25% SoH in Figure 3a exhibits a higher intensity of DEC (at 4.62 min) compared to the TIC of LiClO$_4$ electrolyte from cells cycled to 50% SoH. This confirms the above-mentioned assumption that with longer charge/discharge cycling more transesterification takes place. Furthermore, the LiClO$_4$ electrolyte recovered from cells cycled to 25% SoH contains a higher amount of 'OHCs, namely dimethyl-2,5-dioxahexane dicarboxylate (DMDOHC, 11.37 min), ethyl methyl-2,5-dioxahexane dicarboxylate (EMDOHC, 11.82 min), and diethyl-2,5-dioxahexane dicarboxylate (DEDOHC, 12.21 min), compared to the LiClO$_4$ electrolyte from cells cycled to 50% SoH.

When FEC is added to the electrolyte to form a protective layer on the anode, the amount of DMC, DEC, and 'OHCs in the electrolyte from cells cycled to 50% SoH is reduced. Only a small peak corresponding to FEC (m/z 106, at 6.59 min) is found in the electrolyte, shown in Figure 3b, indicating that the FEC is nearly consumed completely. Thus, after a certain number of charge/discharge cycles, the electrode passivation might no

longer be sufficient to completely suppress the transesterification and 'OHCs formation process. With LiPF$_6$ as conductive salt, the cell cycle life until 50% SoH is prolonged (up to 325–350 cycles), however, the amount of DEC and 'OHCs is still lower compared to the electrolytes containing LiClO$_4$ without FEC. This indicates a better anode surface passivation, hindering transesterification, by the SEI formed with the electrolyte containing PF$_6^-$ compared to ClO$_4^-$. Furthermore, this is in good agreement with the above-mentioned inferior electrochemical performance of the cells with LiClO$_4$. Nevertheless, the higher amount of DEC and 'OHCs in cells with LiPF$_6$ compared to cells with LiClO$_4$+FEC indicates a better surface passivation by the degradation products of FEC.

Interestingly, in the samples containing LiClO$_4$ as conductive salt, chlorinated EMC is found in the cycled electrolytes. Three peaks in the extracted ion chromatogram (EIC) of the fragment m/z 103 and a peak in the EIC of the fragment m/z 110 can be observed in Figure 3b. The characteristic fragments indicate three different chlorinated EMC structures in the electrochemically aged electrolytes, namely 1-chloroethyl methyl carbonate (1-ClE-EMC, m/z 103, 6.18 min), chloromethyl ethyl carbonate (ClM-EMC, m/z 110, 7.50 min), and 2-chloroethyl methyl

Figure 3. a) GC-MS chromatogram with the total ion chromatograms (TICs) of electrolytes with 1.0 M LiPF$_6$, 1.0 M LiClO$_4$, or 1.0 M LiClO$_4$+0.1 M FEC electrochemically aged to 50% or 25% SoH from NMC622‖AG cells with EC/EMC (3:7, by weight). b) Magnification of the TICs in a) in the region 6.0–9.0 min with the extracted ion chromatograms (EICs) of the characteristic fragments of 1-chloroethyl methyl carbonate (1-ClE-EMC, m/z 103, 6.18 min), chloromethyl ethyl carb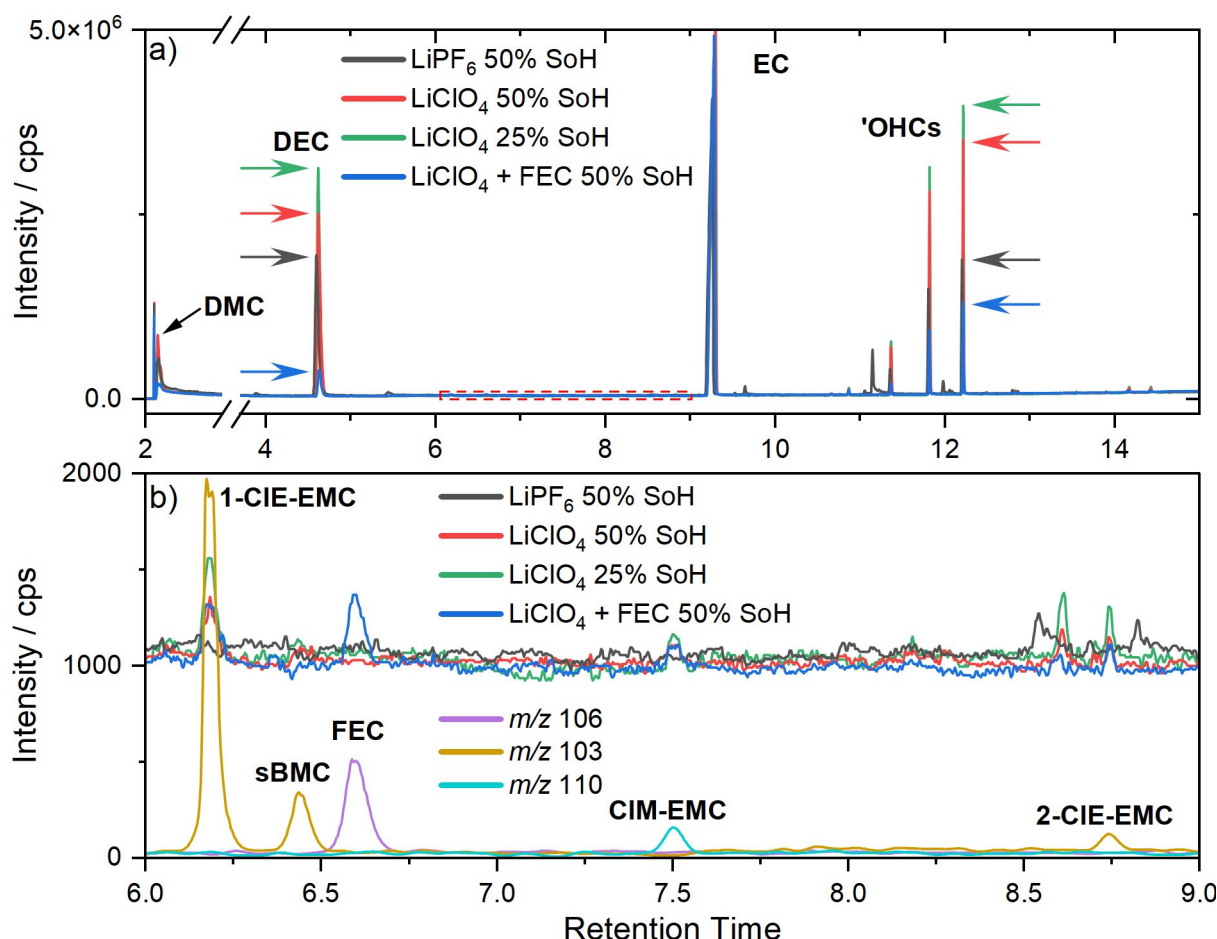onate (ClM–EMC, m/z 110, 7.50 min), and 2-chloroethyl methyl carbonate (2–ClE–EMC, m/z 103, 8.47 min) of chlorinated EMC and FEC (m/z 106, at 6.59 min). Note, that m/z 103 at 6.44 min corresponds to sec-butyl methyl carbonate (sBMC).

carbonate (2-ClE-EMC, m/z 103, 8.47 min). The position of the chlorine is determined by the characteristic fragmentation patterns, shown in Figure S8. The structures of chlorinated EMC products are shown in Figure 4c Note, that m/z 103 at 6.44 min corresponds to *sec*-butyl methyl carbonate (sBMC).[52]

So far, some oxidation mechanisms of the linear carbonates DMC, EMC, and DEC are already reported in the literature, *i.e.* initiated by atmospheric photo-oxidation with chlorine.[53–55] In short, chlorine radicals are formed by photolysis of Cl_2 from the atmosphere, which then can abstract hydrogen to form HCl. Subsequently, the resulting organic carbonate radicals can either recombine or react with chlorine or oxygen to form peroxo-radicals.[53–55] Also, different pathways of chlorination by electrocatalysis have already been reported, *i.e.* with $MnCl_3$ as a chlorination agent.[56,57] However, initially only perchlorate anions are present in the pristine electrolyte. Thus, chlorine
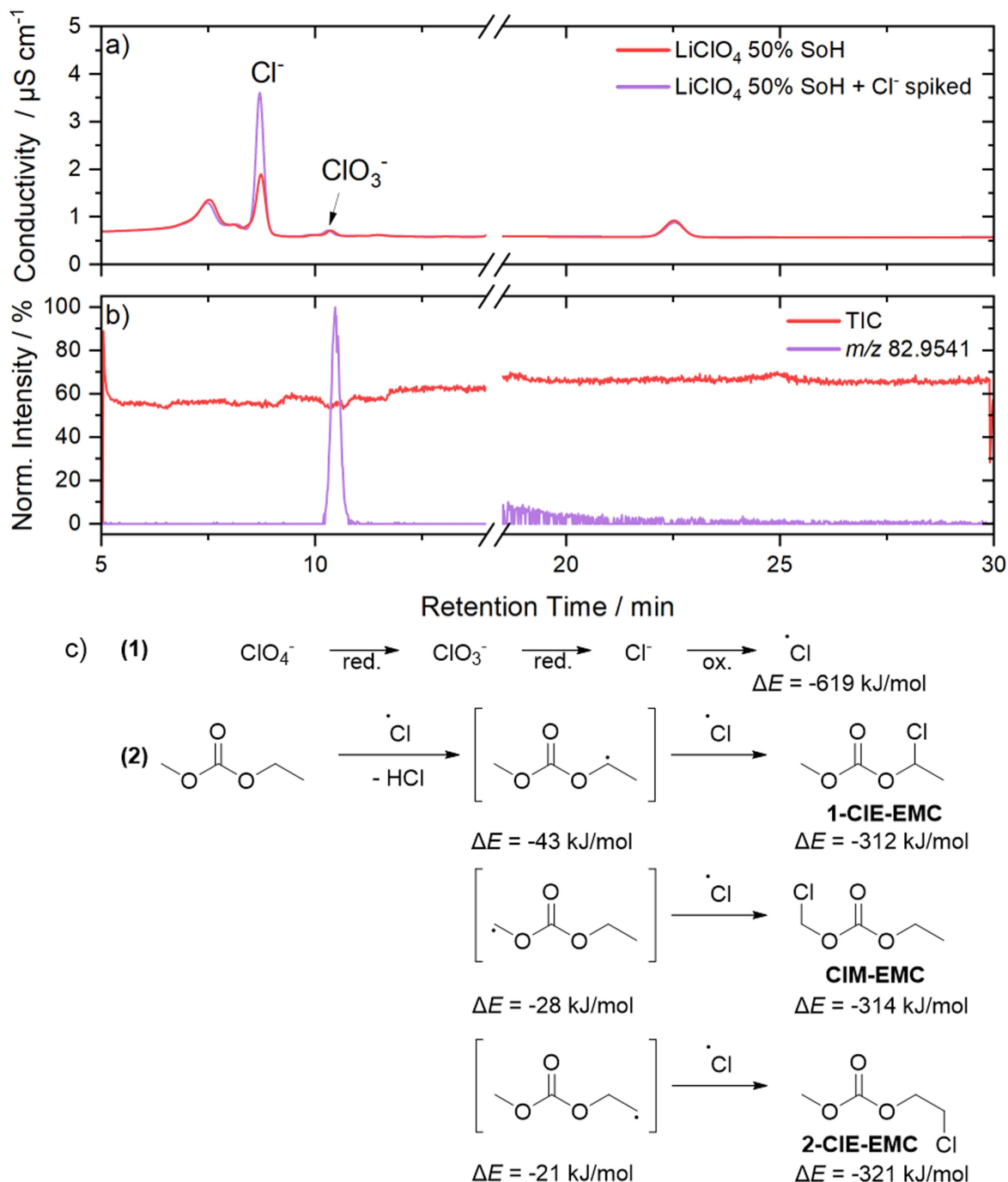

Figure 4. a) Conductivity and b) mass spectrometry chromatogram obtained by ionic conductivity-conductivity detection-mass spectrometry (IC–CD-MS) of 1.0 M $LiClO_4$ in EC/EMC from NMC622||AG cells cycled to 50% SoH. Chloride spiking of the electrolyte was performed as an internal reference. c) putative reaction (1) from perchlorate to chlorine radical and (2) dehydrogenation of EMC at the methyl or ethyl group positions by chlorine radical under HCl formation and subsequent addition of a chlorine radical. Reduction and oxidation are abbreviated with red. and ox., respectively.

Batteries & Supercaps

Research Article
doi.org/10.1002/batt.202400568

Chemistry Europe
European Chemical
Societies Publishing

radicals need to be formed by perchlorate reduction. As already reported in previous studies, perchlorate can be reduced on the cathode to chlorate, which can then rapidly be reduced to chloride.[32,58] Furthermore, the reduction potential from molten chlorate to chloride was found to be 3.24 V $vs.$ Li|Li$^+$, which is in the operational voltage range of the cells used in this study, considering a similar potential of lithiated graphite to lithium metal.[59]

The presence of chloride and chlorate species in the electrochemically aged electrolytes is analyzed through IC–CD-MS and the respective chromatograms are shown in Figure 4a and b. Due to a mass threshold of $m/z = 70$ of the mass spectrometer, chloride is not included in the MS chromatogram in Figure 4b. Thus, the electrochemically aged electrolyte with LiClO$_4$ was measured with and without chloride spiking to confirm the presence of chloride via conductivity detection (Figure 4a). The conductivity chromatogram in Figure 4a exhibits a conductivity increase of the peak at 8.73 min in the case of the chloride-spiked electrolyte compared to the non-spiked electrolyte. Thus, this peak is assigned to chloride. The peak corresponding to chlorate in the conductivity chromatogram is identified by comparison with the corresponding mass ($m/z = 82.9541$) in the MS chromatogram in Figure 4b. A retention time of 10.45 min is found for chlorate. Compared to chloride, the amount of chlorate is determined to be much lower in the electrolyte, as shown in the conductivity chromatogram in Figure 4a. This indicates a faster reaction from chlorate to chloride than from perchlorate to chlorate, which is in good agreement with previous studies.[32,58]

The underlying putative reaction mechanisms are given in the scheme in Figure 4c, with the reduction from perchlorate to chlorine radicals in (1), and the hydrogen abstraction by a chlorine radical with the subsequent chlorination of EMC (2). By DFT calculations, the ΔE for the hydrogen abstraction and the formation of a radical at the CH$_3$ groups of the methyl ($\Delta E = -28$ kJ mol^{-1}) and ethyl ($\Delta E = -21$ kJ mol^{-1}) are calculated. For the hydrogen abstraction and the formation of a radical at the CH$_2$ group of the ethyl chain a ΔE of -43 kJ mol^{-1} is calculated, indicating a preferred reaction at this position. Additionally, the energy gain of the formation of 1-ClE-EMC results in an overall ΔE of -355 kJ mol^{-1} compared to -342 kJ mol^{-1} for the formation of ClM-EMC and 2-ClE-EMC. This is in good agreement with the results of the IC–CD-MS analysis (Figure 3b), showing a much higher peak for 1-ClE-EMC compared to ClM-EMC and 2-ClE-EMC. Furthermore, the intensity of the peak corresponding to ClM-EMC is slightly higher compared to the peak of 2-ClE-EMC, which is also in agreement with the slightly higher energy gain for the radical formation at the methyl group. The impact of the chlorinated EMC products on the electrochemical performance remains unclear. Furthermore, due to the relatively low amount of the formed chlorinated EMC in the cells in this study, a beneficial, detrimental, or non-existent impact on the overall performance in this study might be insignificant. Nevertheless, similar to fluorinated carbonates, the chlorinated EMC products might offer different (electro−)chemical or passivating properties compared to the non-halogenated counterparts and thus be beneficial for high-voltage applications.[60,61] Preliminary DFT calculations show that the chlorination of EMC weakens the C−O bond and that these molecules exhibit lower LUMOs (lowest unoccupied molecular orbitals), suggesting a reduction of chlorinated EMC before EMC (see Table S1, Supplementary Information).

Interestingly, the above-mentioned chlorinated EMC derivatives were already found as degradation products in a previous study by our group using the same NMC622||AG cell setup.[62] However, in that study, chloroethylene carbonate was used as electrolyte additive for SEI formation, and the chlorinated EMC derivatives were not formed with a radical intermediate on the cathode, as shown in the scheme in Figure 4c, but simply by EC ring opening and transesterification on the anode.

2.3. Electrode Investigation

To gain deeper insights into the morphology and surface elemental composition of the aged electrodes from the cells cycled with LiClO$_4$ and LiClO$_4$+FEC electrolyte, (FIB−)SEM and EDX spectroscopy measurements were carried out. The investigation of the anodes reveals no major morphological differences between the formed SEIs with LiClO$_4$ and LiPF$_6$ (Figure S9). However, on the surface of the cathode cycled in a cell with LiClO$_4$-based electrolyte (Figure 5a and b), two different types of deposits are visible - smaller (d < 50 μm) and more spherical ones and larger (d > 50 μm) more irregularly shaped ones. This might indicate two different originations or formation mechanisms of these particles. With SEM1 (Figure 5c) and light microscopy with a confocal Raman spectrometer (Figure S10) different shapes for the larger deposits were found. Generally, the observed deposits were not removable by washing with DMC.

The deposits in Figure 5b and c are located on top of the surface of the cathode active material. As this may clog underlying pores in the cathode active material, which are necessary for proper electrolyte diffusion, these deposits may cause decreasing cathode capacities by deactivating NMC particles. This assumption is in good agreement with the faster-decreasing discharge capacities of the cells with LiClO$_4$ compared to cells with LiPF$_6$. The deposits are also found on cathodes from cells cycled with LiClO$_4$ and FEC-containing electrolyte, but they are not found with the other investigated lithium salts with PF$_6^-$, TFSI$^-$, BOB$^-$, or BF$_4^-$ (Figure S11). The additional (FIB−)SEM and EDX spectroscopy measurements are shown in Figure S12.

FIB-SEM and EDX spectroscopy are utilized for cutting and elementary analyzing the two types of deposits to unravel the elemental composition. As shown in Figure 5d and e, these deposits are largely formed by composite containing at least aluminum, oxygen, and chlorine. Most likely, lithium is included in the structures, but lithium cannot be detected by EDX. However, determining the accurate Al:O:Cl ratio of the composite employing EDX is ambiguous, as degradation products, originating from the electrolyte components EC, EMC, or LiClO$_4$, might be included in the obtained EDX spectra.

Batteries & Supercaps

Research Article
doi.org/10.1002/batt.202400568

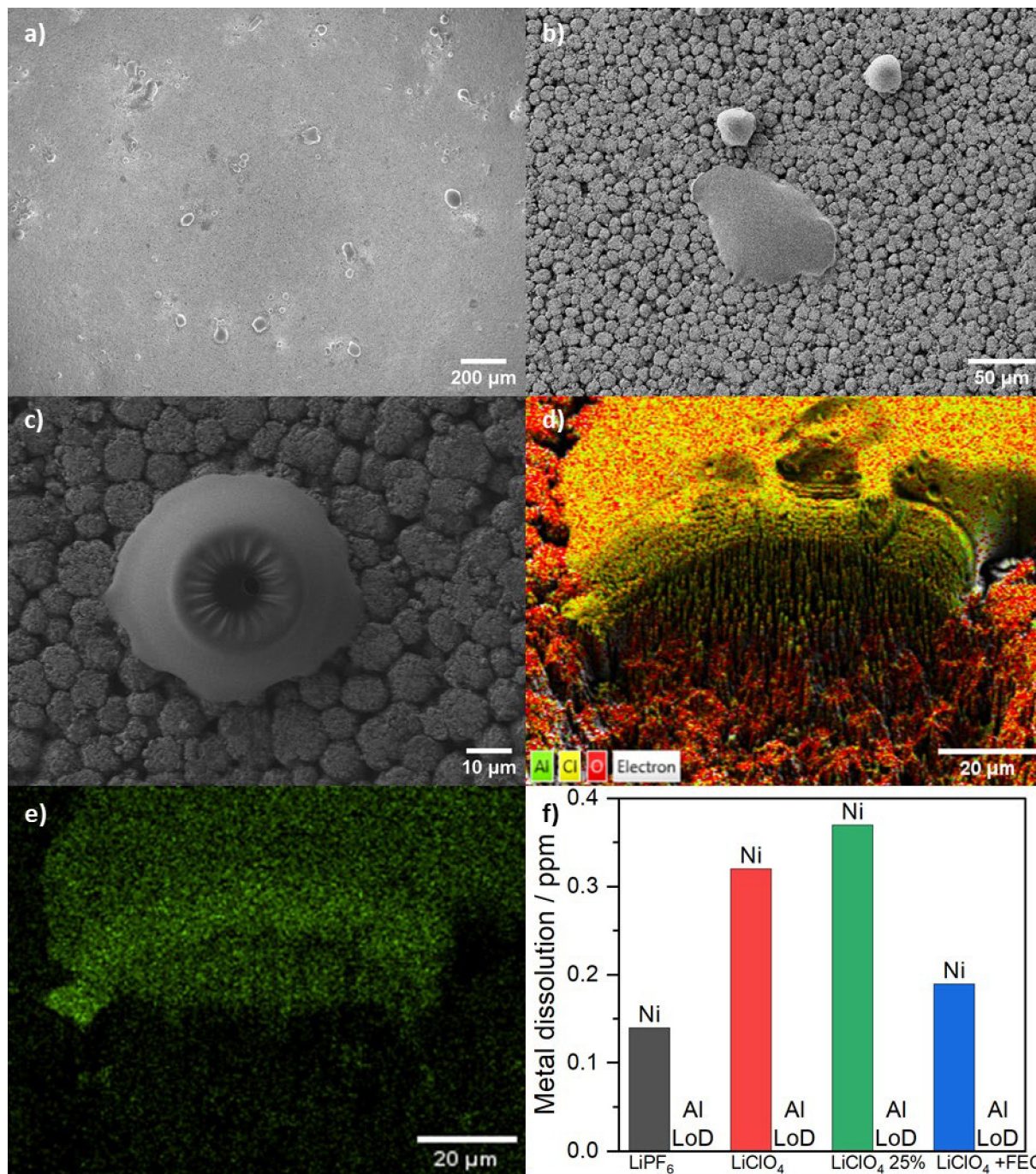**Chemistry Europe**
European Chemical
Societies Publishing

Figure 5. SEM images of the cathodes collected from NMC622||AG cells cycled with LiClO₄-containing electrolyte to 50 % state-of-health, obtained with SEM 2 if not stated otherwise. a) and b) washed cathode obtained, c) washed cathode (SEM 1), d) side view obtained by FIB cutting of a deposit with EDX overlay, e) Al EDX detections in d), f) TXRF detections of Ni and Al in the corresponding electrolytes.

As the elemental analysis by EDX is not straightforward, the deposits are additionally investigated on a molecular level by Raman microscopy to analyze the composition (Figures S10 and S13). The Raman spectra of the deposits on the cathodes reveal bands around 460 cm^{-1}, 628 cm^{-1}, and 932 cm^{-1}, which can be assigned to δ_{asym}(Cl–O), δ_{sym}(Cl–O), and ν_{sym}(Cl–O) vibrations of the perchlorate anion in aluminum perchlorate.[63] Comparing the literature spectra of different metal-perchlorates and -chlorates, the respective bands of chlorate in the obtained spectra may be overlapped by the perchlorate bands.[63] Furthermore, some chlorate salts exhibit an additional feature around 980 cm^{-1}.[63] However, pure aluminum chlorate as a reference or a Raman spectrum in the literature is not available, thus identification and semi-quantification are not possible. Furthermore, a clear and correct distinction might not be accurate, due to the additional lithium in the Li$_w$Al$_x$O$_y$Cl$_z$ composite deposits, which may cause a blue shift.[63] Besides perchlorate and chlorate, electrolyte residues could be a

Batteries & Supercaps

Research Article
doi.org/10.1002/batt.202400568

Chemistry Europe
European Chemical
Societies Publishing

plausible assignment for the observed bands. A comparison with spectra of electrolyte solvents EC and EMC and 'OHCs as typical degradation products shows no matching bands, excluding those molecules as origins of the bands (Figure S13). Whereas lithium, oxygen, and chlorine are most likely originating from the electrolyte, the aluminum could originate from the anodic dissolution of the current collector or the aluminum oxide ceramic coating on the cathode side of the separator.[64–68] To address this, TXRF spectroscopy is utilized to quantify the aluminum in the electrolyte. Albeit there are many large $(Li_x)Al_xO_yCl_z$ composite deposits on the cathodes cycled with $LiClO_4$-based electrolytes, aluminum is below the limit of detection in the corresponding extracted aged electrolytes (Figure 5f). This leads to the conclusion that aluminum is directly complexed and sedimented on the cathode.

Additionally, by TXRF spectroscopy nickel is found in the electrolytes with $LiPF_6$, $LiClO_4$, and $LiClO_4 + FEC$, indicating transition metal dissolution from the cathode active material by HF or HCl.[69] The lowest amount of nickel is found when $LiPF_6$ is used as conductive salt (0.14 ppm), followed by the electrolyte containing $LiClO_4 + FEC$ (0.19 ppm) and the electrolyte containing $LiClO_4$ (0.32 ppm). When extending the cycle life of cells with the $LiClO_4$ electrolyte from 50% to 25% SoH, the amount of nickel found in the electrolyte increases to 0.37 ppm. The higher quantity of nickel in the electrolytes with $LiClO_4$ and $LiClO_4 + FEC$ compared to $LiPF_6$, although the cycle life of the cells with $LiPF_6$ electrolyte is much longer. This could either indicate a higher rate of TM dissolution with HCl than with HF

or a better TM scavenging effect of fluorophosphates compared to perchlorate or chlorate species.

The findings in the presented study are presented schematically in Figure 6, showing the deposition of $(Li_w)Al_xO_yCl_z$, degradation of perchlorate to chlorate and chloride, chlorination of EMC, transesterification of EMC to DMC and DEC, and formation of 'OHCs.

3. Conclusion & Outlook

In this study, $LiClO_4$ is re-visited as a fluorine-free conductive salt for high-voltage application in NMC622||AG cells and compared to electrolytes with $LiPF_6$ and $LiClO_4 + FEC$. In terms of capacity retention, internal resistance, and Coulombic efficiency, the electrochemical performance of cells containing $LiClO_4$ can be increased by the addition of FEC. However, cells with either of both electrolyte formulations exhibit inferior electrochemical performance compared to $LiPF_6$. The investigation of the electrochemically aged electrodes and electrolytes reveals the formation of chloride and chlorate anions via perchlorate reduction and chlorination of EMC at the methyl and both ethyl positions during high-voltage operation. This is likely caused by the formation of chlorine radicals at the cathode. Furthermore, the sedimentation of $(Li_w)Al_xO_yCl_z$ composite is found on the cathodes from cells containing $LiClO_4$, including perchlorate and chlorate species. These deposits were found to differ in shape and size, ranging from 20–200 μm. Furthermore, the quantity of dissolved aluminum and nickel in
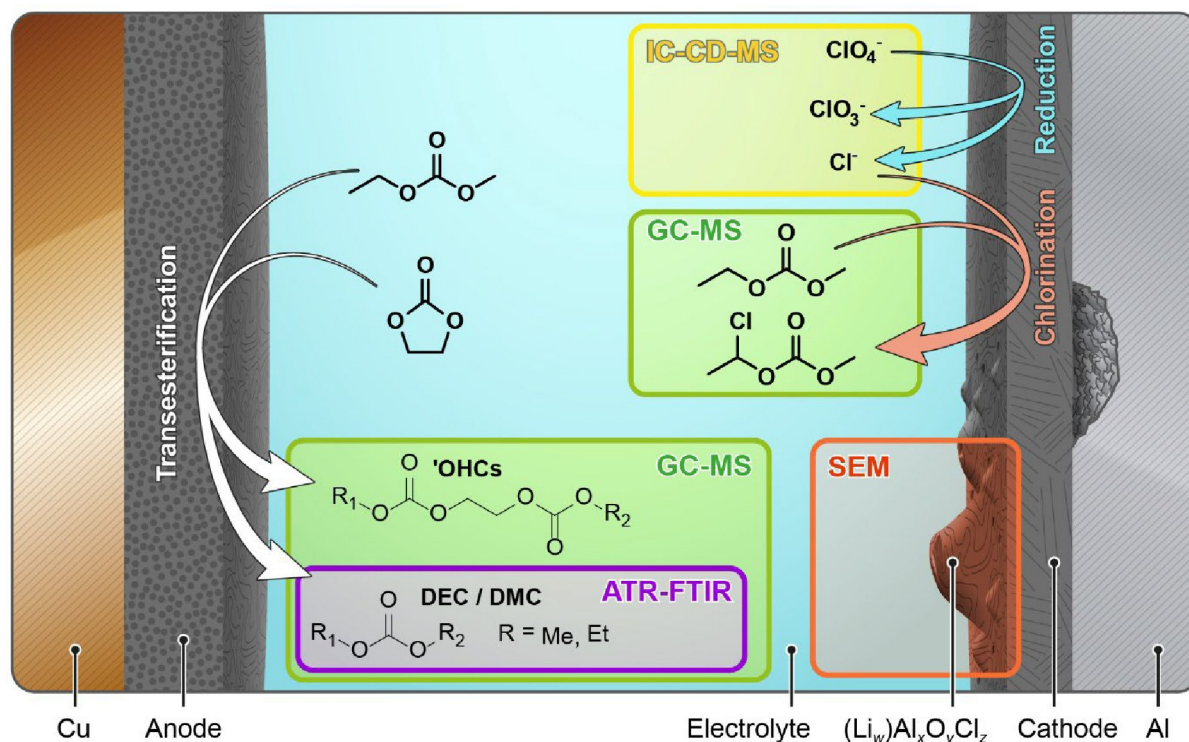

Figure 6. Schematic depiction of the transesterification and 'OHCs formation detected with GC-MS and ATR-FTIR on the anode, reduction from perchlorate to chlorate and chloride detected with IC–CD-MS, chlorination of EMC detected with GC-MS, and deposition of $(Li_w)Al_xO_yCl_z$ composite detected with (FIB−)SEM on the cathode.

Batteries & Supercaps

Research Article
doi.org/10.1002/batt.202400568

Chemistry Europe
European Chemical
Societies Publishing

the electrolyte is investigated, showing a higher amount of nickel in the electrolyte from cells with $LiClO_4$ compared to $LiPF_6$. Contrary to nickel, aluminum is not detected in the electrolytes from the cells containing $LiPF_6$ or $LiClO_4$, indicating a direct sedimentation by chlorate or perchlorate forming $(Li_w)Al_xO_yCl_z$. Overall, the observed aging mechanisms lead to increased cell resistance, reduced capacity retention, and accelerated degradation of the $LiClO_4$-containing electrolytes compared to the $LiPF_6$-containing counterpart.

To tackle the observed failure phenomena, follow-up studies might focus on enhanced electrode passivation and interphase formation to suppress chemical and electrochemical degradation. This can relatively straightforwardly be achieved through the utilization of functional electrolyte additives, as shown in different studies using the same or similar cells.[10,11,37,50,62,70,71] Regarding the suppression of transesterification and the formation of 'OHCs at the anode, FEC as anode-functional electrolyte additive is fulfilling this role in this study. As FEC contains fluorine, fluorine-free additives such as vinylene carbonate, chloroethylene carbonate, or 2-sulfobenzoic acid anhydride are promising substitutes.[37,62] Furthermore, the formation of a sufficient interphase on the cathode might hinder chlorate, chloride, and chlorine-radical formation. This could be achieved by non-fluorinated electrolyte additives such as vinylethylene carbonate, thiophene, or thiophene boronic acid.[10,11,62] Also, passivation of the aluminum current collector should be addressed by incorporating alternative salts to suppress aluminum dissolution and therefore the sedimentation of $(Li_w)Al_xO_yCl_z$ deposits. To investigate the chlorinated EMC degradation products toward their influence under real working conditions in battery cells, follow-up studies might address chlorinated EMC as an electrolyte co-solvent or additive in high-voltage cells.

Experimental

Electrolyte Preparation

$LiPF_6$ and $LiClO_4$ were purchased from E-Lyte Innovations GmbH and dried at 80 °C under reduced pressure (0.05 mbar). The electrolytes were prepared by dissolving each 1.0 M of $LiPF_6$ or $LiClO_4$ in EC/EMC 3:7 (by weight, purchased from E-Lyte Innovations GmbH). A concentration of 0.1 M FEC (abcr GmbH) was used in the additive-containing electrolyte with $LiClO_4$. All electrolytes were prepared in an Ar-filled glovebox (MBraun) with H_2O and O_2 values below 10 ppm.

Electrochemical Investigation

Galvanostatic charge/discharge cycling experiments were conducted with commercially available multilayer pouch cells with NMC 622∥ AG electrodes (nominal capacity of 200 mAh, cycled between 2.8–4.5 V) by Li-FUN Technologies Corporation Limited (Zhuzhou, China), which were received without electrolyte. The pouch cells were cut open and dried at 80 °C under vacuum (0.05 mbar) for two days. Afterward, the cells were filled with 700 μL of electrolyte and sealed with a GN-HS350 V (Gelon Lib Co., Ltd., China) vacuum sealer at a relative pressure of 15% of the ambient pressure in a dry-room (dew-point: < −50 °C). The cells

were clamped with a force of 0.46 Nm onto a specifically designed cell holder to apply a pressure of about 2 bar, and constant current charge/discharge cycled using a Maccor Series 4000 battery testing unit (Maccor Inc., US) in a temperature-controlled chamber (Binder) at 20 °C. Further details regarding the specifically designed cell holder can be found in a previous publication by Schmiegel et al.[72] The electrochemical investigation started with an OCV step to ensure proper electrode wetting for 24 h. Cell formation was performed by three charge/discharge cycles at 0.1 C and 0.3 C each. Afterward, the pouch cells were cut open and re-sealed at the electrode stack ("degassing") under the above-mentioned conditions. The cells were then reconnected and charge/discharge cycled at 1 C in a voltage range of 4.5–2.8 V until 80% state-of-health (SoH, 80% of the capacity compared to the first cycle at 1 C) was reached. An average of 4 cells was taken for each investigated electrolyte formulation. Additional storage experiments to investigate the self-discharge of the cells with the used electrolyte formulations, similar to Metzger et al., are shown in Figure S3 in the Supporting Information.[73–76]

Electrode and Electrolyte Characterization

Extraction of Electrochemically Aged Electrolytes

To obtain electrochemically aged electrodes and electrolytes, the galvanostatically cycled pouch cells at 50% or 25% SoH were opened in a glovebox (O_2, H_2O contents < 0.1 ppm), and the electrolytes were extracted via centrifugation of the anode and separator.

Infrared Spectroscopy

Fourier-transform infrared (FTIR) spectroscopy investigations were performed with an Invenio-R spectrometer (Bruker) with a Platinum ATR unit (Diamond crystal, Bruker) in a N_2-flushed custom-built glovebox. Spectra of the pristine and electrochemically aged liquid electrolyte samples on the ATR crystal were collected at a resolution of 4 cm^{-1} by accumulating 32 background and 32 sample scans with an MCT detector. Additional rubberband correction with 15 iterations (straight lines) was performed.

Morphological Investigations

The electrode morphology was investigated using a scanning electron microscope (SEM, Zeiss Auriga Crossbeam Workstation) equipped with a Schottky-type field emission gun and an energy-dispersive X-ray spectroscopy system (EDX, X–Max 80 mm2 detector, Oxford Instruments). The images were acquired using an acceleration voltage of 3 kV and 20 kV for EDX with a working distance of ≈5 mm. Before SEM measurements, some electrodes were rinsed with dimethyl carbonate and dried under reduced pressure. The corresponding pictures are labeled with washed or unwashed. This is later referred to as SEM1.

Due to the technical limitations of SEM1 regarding sample cutting via focused ion beam (FIB), additional SEM images were obtained by a Zeiss Crossbeam 550 electron microscope (Carl Zeiss Microscopy GmbH). Images were taken at 3 kV accelerating voltage and with an aperture size of 30 μm using an in-lens detector with a working distance of ≈5 mm. The acquisition time was optimized so that the electron beam did not induce any surface changes during exposure at high magnifications. To prevent air exposure, all samples were transferred using a vacuum-sealed sample holder.

Batteries & Supercaps

Research Article
doi.org/10.1002/batt.202400568

Chemistry Europe
European Chemical
Societies Publishing

The focused ion beam (FIB, Zeiss Ion sculptor FIB-column; Carl Zeiss Microscopy GmbH) was employed to cut the electrodes. Energy dispersive X-ray spectroscopy with an acceleration voltage of 5 kV was measured with an Ultim Extreme detector to evaluate the elemental composition of the samples. The spectra were evaluated with the Integrated Calibration and Application Tool (INCA) software (Oxford Instruments). Prior to SEM measurements, some electrodes were dried under reduced pressure. After the first set of measurements, some electrodes were rinsed with dimethyl carbonate prior to a second measurement. The corresponding pictures are labeled with washed or unwashed. This is later referred to as SEM2.

Gas Chromatography-Mass Spectrometry

A qualitative analysis of volatile electrolyte species was executed on a GCMS-QP2010 Ultra (Shimadzu) equipped with a non-polar Restek Rxi®-5 ms (30 m×0.25 mm×0.25 μm) fused silica column (5% diphenyl/ 95% dimethyl polysiloxane). The sample injection was done with a volume of 1 μL at an applied split ratio of 1:20 and a set temperature of 250 °C. Helium (6.0 purity) was used as carrier gas with a column flow of 1.15 mL min^{-1}. The oven program started with an initial temperature of 40 °C which was held for 1 min, followed by a first ramp of 3 °C min^{-1} to 60 °C and a subsequent second ramp of 30 °C min^{-1} until a temperature of 260 °C was reached. This final temperature was held for 2 min, resulting in a total measurement time of 16.33 min. The MS operated in the electron ionization (EI) mode with an ion source temperature of 200 °C and an interface temperature of 250 °C, while the filament voltage was set to 70 V and the detector voltage was relative to the respective tuning file. The mass range was set to 30–350 m/z with an event time of 0.1 s in scan mode. If possible, the identification of compounds was verified with the NIST 11 library. All samples were diluted 1:100 with DCM to precipitate and remove the conductive salt prior to injection.

Ion Chromatography-Conductivity Detection-Mass Spectrometry

A qualitative analysis of anionic species in the extracted electrolyte was executed on an 850 Professional IC (Metrohm, Switzerland) with conductivity detection (CD) hyphenated to a 6530 Accurate Mass Quadrupole-Time-of-Flight (Q-TOF)-MS (Agilent, USA). A Metrosep A Supp 7 column (250×4.0 mm, 5 μm; Metrohm) with a Metrosep A Supp 5 Guard/4.0 guard column was used for an isocratic separation of the anionic compounds at an oven temperature of 65 °C and an applied flow rate of 0.7 mL min^{-1} over a total runtime of 30 min. All samples were diluted 1:100 with acetonitrile and the injection volume was set to 65 μL. The eluent consisted of a 3.6/3.4 mM Na$_2$CO$_3$/NaHCO$_3$ aqueous solution and acetonitrile in a ratio of 58:42 (v/v). The utilized suppressor was sequentially regenerated by 0.1 M sulfuric acid and rinsed with MilliQ water. Ionization in the MS was performed in ESI(−) mode at a capillary voltage of 3.5 kV. The nebulizer gas was set to 45 psig and drying gas to a flow of 10 L min^{-1} at 350 °C. A collision-induced dissociation energy of 30 eV was applied for MS/MS experiments and the mass range was set to m/z 70–500 in MS^1 and m/z 50–500 in MS^2. Instrument control, data acquisition, and data evaluation were performed for MS with MassHunter Data Acquisition and MassHunter Qualitative Analysis B.08.00 (Agilent), while for IC with MagIC Net 3.3 (Metrohm).

Density Functional Theory Calculations

Density functional theory (DFT) calculations were carried out using the Gaussian16 package.[77] All geometries were optimized using B3LYP DFT functional and the 6–311++G(3df, 2p) basis set. The effect of a surrounding electrolyte was mimicked by SMD implicit solvation model using parameters for acetone, showing a similar dielectric constant as liquid carbonate-based electrolytes.[10,37,78–80] The electronic energies for the putative reactions were calculated with thermal energy correction (298.15 K).

Raman Spectroscopy

Raman spectroscopy measurements were carried out using a confocal Raman microscope (Horiba Scientific, LabRAM HR evolution, air-cooled CCD detector, 600 g mm^{-1} grating). The samples were excited by a green laser (532 nm) with a power output of 34 mW at the objective. The laser power was adjusted accordingly using a 10% or 1% filter. The laser was focused by a 50× long-working distance objective (Carl Zeiss Microscopy, 9.2 mm, numerical aperture 0.5). Raman spectra were recorded by three integrations of 35 s. The Raman spectrometer, data acquisition, and analysis were handled using LabSpec 6.7.1.10 (Horiba Scientific).

Total Reflection X-Ray Fluorescence (TXRF) Spectroscopy

A S2 PICOFOX system (Bruker Corporation, Billerica, USA) was used for determining transition metal contents in electrolyte solutions. All measurements were carried out on 30 mm quartz glass carriers from Bruker Corporation, which were pre-treated with a silicon solution (SERVA Electrophoresis GmbH, Heidelberg, Germany) for ensuring hydrophobic surface properties. The measurement was set at 600 s irradiation per sample. Further parameters and sample preparation conditions were applied according to Evertz et al.[81]

Supporting Information Summary

Supporting Information is available from the Wiley Online Library or from the author.

Conflict of Interests

The authors declare no conflict of interest.

Data Availability Statement

The data that support the findings of this study are available from the corresponding author upon reasonable request.

[1] K. Itani, A. De Bernardinis, *Energies* **2023**, *16*(22).
[2] X. Zeng, M. Li, D. Abd El-Hady, W. Alshitari, A. S. Al-Bogami, J. Lu, K. Amine, *Adv. Energy Mater.* **2019**, *9* (27), 1900161.
[3] G. Bridge, E. Faigen, *Energy Res. Social Sci.* **2022**, *89*, 102659.
[4] J. Liu, Z. Bao, Y. Cui, E. J. Dufek, J. B. Goodenough, P. Khalifah, Q. Li, B. Y. Liaw, P. Liu, A. Manthiram, Y. S. Meng, V. R. Subramanian, M. F. Toney, V. V. Viswanathan, M. S. Whittingham, J. Xiao, W. Xu, J. Yang, X.-Q. Yang, J.-G. Zhang, *Nat. Energy* **2019**, *4*(3), 180–186.
[5] P. Liu, S. Meng, *Battery500 Consortium: Development of High Capacity Cathodes and Robust Solid Electrolytes*, Univ. of California, San Diego, CA, United States **2022**.
[6] K. Edström, **2020**.
[7] L. Ibing, T. Gallasch, P. Schneider, P. Niehoff, A. Hintennach, M. Winter, F. M. Schappacher, *J. Power Sources* **2019**, *423*, 183–191.
[8] S. Klein, P. Bärmann, T. Beuse, K. Borzutzki, J. E. Frerichs, J. Kasnatscheew, M. Winter, T. Placke, *ChemSusChem* **2021**, *14*(2), 595–613.
[9] M. Singh, J. Kaiser, H. Hahn, *Batteries* [Online], **2016**.
[10] F. Pfeiffer, D. Diddens, M. Weiling, L. Frankenstein, S. Kühn, I. Cekic-Laskovic, M. Baghernejad, *Adv. Energy Mater.* **2023**, *13*(25), 2300827.
[11] F. Pfeiffer, D. Diddens, M. Weiling, M. Baghernejad, *ACS Appl. Mater. Interfaces* **2023**, *15*(5), 6676–6686.
[12] F. Demelash, A. Gomez-Martin, B. Heidrich, E. Adhitama, P. Harte, A. Javed, A. Arifiadi, M. M. Bela, P. Yan, P. Harte, D. Diddens, M. Winter, P. Niehoff, *Small Struct.* **2024**, *n/a(n/a)*, 2400063.
[13] S. Klein, P. Harte, S. van Wickeren, K. Borzutzki, S. Röser, P. Bärmann, S. Nowak, M. Winter, T. Placke, J. Kasnatscheew, *Cell Rep. Phys. Sci.* **2021**, *2*(8), 100521.
[14] I. Buchberger, S. Seidlmayer, A. Pokharel, M. Piana, J. Hattendorff, P. Kudejova, R. Gilles, H. A. Gasteiger, *J. Electrochem. Soc.* **2015**, *162*(14), A2737.
[15] X. Ma, J. E. Harlow, J. Li, L. Ma, D. S. Hall, S. Buteau, M. Genovese, M. Cormier, J. R. Dahn, *J. Electrochem. Soc.* **2019**, *166*(4), A711.
[16] J. Kalhoff, G. G. Eshetu, D. Bresser, S. Passerini, *ChemSusChem* **2015**, *8*(13), 2154–2175.
[17] P. Molaiyan, S. Bhattacharyya, G. S. dos Reis, R. Sliz, A. Paolella, U. Lassi, *Green Chem.* **2024**, *26*(13), 7508–7531.
[18] S. Klein, L. Haneke, P. Harte, L. Stolz, S. van Wickeren, K. Borzutzki, S. Nowak, M. Winter, T. Placke, J. Kasnatscheew, *ChemElectroChem* **2022**, *9*(13), e202200469.
[19] M. Kubot, L. Frankenstein, E. Muschiol, S. Klein, M. Esselen, M. Winter, S. Nowak, J. Kasnatscheew, *ChemSusChem* **2023**, *16*(6), e202202189.
[20] N. von Aspern, G. V. Röschenthaler, M. Winter, I. Cekic-Laskovic, *Angew. Chem. Int. Ed.* **2019**, *58*(45), 15978–16000.
[21] G. Hernández, R. Mogensen, R. Younesi, J. Mindemark, *Batteries Supercaps* **2022**, *5*(6), e202100373.
[22] K. Asheim, I. F. Holsen, V. Renmann, M. V. Blanco, P. E. Vullum, N. P. Wagner, J. P. Mæhlen, A. M. Svensson, *Batteries Supercaps* **2024**, *7*(6), e202300541.
[23] J. Qiu, J. Guo, J. Li, Y. Wu, Z. Fan, H. Ye, Z. Fang, Z. Zhang, R. Zeng, *ACS Appl. Mater. Interfaces* **2023**, *15*(49), 56918–56929.
[24] S. Yuan, S. Cao, X. Chen, J. Wei, Z. Lv, H. Xia, J. Li, H. Zhang, L. Liu, C. Tian, L. Chen, W. Zhang, Z. Xing, H. Li, S. Li, Q. Zhu, X. Feng, X. Chen, *Adv. Mater.* **2024**, *36*(16), 2311327.
[25] K. Xu, *Chem. Rev.* **2004**, *104*(10), 4303–4418.
[26] K. Xu, *J. Electrochem. Soc.* **2008**, *155*(10), A733.
[27] K. Xu, B. Deveney, K. Nechev, Y. Lam, T. R. Jow, *J. Electrochem. Soc.* **2008**, *155*(12), A959.
[28] Z. Liu, J. Chai, G. Xu, Q. Wang, G. Cui, *Coord. Chem. Rev.* **2015**, *292*, 56–73.
[29] R. Marom, O. Haik, D. Aurbach, I. C. Halalay, *J. Electrochem. Soc.* **2010**, *157*(8), A972.
[30] K. Kanamura, *J. Power Sources* **1999**, *81–82*, 123–129.
[31] C. Iwakura, Y. Fukumoto, H. Inoue, S. Ohashi, S. Kobayashi, H. Tada, M. Abe, *J. Power Sources* **1997**, *68*(2), 301–303.
[32] M. Metzger, P. Walke, S. Solchenbach, G. Salitra, D. Aurbach, H. A. Gasteiger, *J. Electrochem. Soc.* **2020**, *167*(16), 160522.
[33] B. Markovsky, F. Amalraj, H. E. Gottlieb, Y. Gofer, S. K. Martha, D. Aurbach, *J. Electrochem. Soc.* **2010**, *157*(4), A423–A423.
[34] M. Koltypin, D. Aurbach, L. Nazar, B. Ellis, *Electrochem. Solid-State Lett.* **2007**, *10*(2), A40.
[35] K. Amine, J. Liu, I. Belharouak, *Electrochem. Commun.* **2005**, *7*(7), 669–673.
[36] G. H. Newman, R. W. Francis, L. H. Gaines, B. M. L. Rao, *J. Electrochem. Soc.* **1980**, *127*(9), 2025.
[37] M. Weiling, C. Lechtenfeld, F. Pfeiffer, L. Frankenstein, D. Diddens, J.-F. Wang, S. Nowak, M. Baghernejad, *Adv. Energy Mater.* **2024**, *14*(5), 2303568.
[38] A. Ghaur, C. Peschel, I. Dienwiebel, L. Haneke, L. Du, L. Profanter, A. Gomez-Martin, M. Winter, S. Nowak, T. Placke, *Adv. Energy Mater.* **2023**, 2203503.
[39] J. C. Burns, N. N. Sinha, G. Jain, H. Ye, C. M. VanElzen, W. M. Lamanna, A. Xiao, E. Scott, J. Choi, J. R. Dahn, *J. Electrochem. Soc.* **2012**, *159*(7), A1105–A1105.
[40] L. Haneke, J. E. Frerichs, A. Heckmann, M. M. Lerner, T. Akbay, T. Ishihara, M. R. Hansen, M. Winter, T. Placke, *J. Electrochem. Soc.* **2020**, *167*(14), 140526.
[41] P. Lanz, P. Novák, *J. Electrochem. Soc.* **2014**, *161*(10), A1555.
[42] A. K. Das, B. N. Rajasekhar, S. Krishnakumar, *J. Quant. Spectrosc. Radiat. Transfer* **2018**, *217*, 53–62.
[43] J. Wang, Y. Wu, X. Xuan, H. Wang, *Spectrochim. Acta, Part A* **2002**, *58*(10), 2097–2104.
[44] B. P. Kar, N. Ramanathan, K. Sundararajan, K. S. Viswanathan, *J. Mol. Struct.* **2014**, *1072*, 61–68.
[45] J. E. Katon, M. D. Cohen, *Can. J. Chem.* **1975**, *53*(9), 1378–1386.
[46] H. Yoshida, T. Fukunaga, T. Hazama, M. Terasaki, M. Mizutani, M. Yamachi, *J. Power Sources* **1997**, *68*(2), 311–315.
[47] L. Madec, R. Petibon, K. Tasaki, J. Xia, J. P. Sun, I. G. Hill, J. R. Dahn, *Phys. Chem. Chem. Phys.* **2015**, *17*(40), 27062–27076.
[48] R. Petibon, J. Xia, J. C. Burns, J. R. Dahn, *J. Electrochem. Soc.* **2014**, *161*(10), A1618.
[49] F. Horsthemke, M. Leißing, V. Winkler, A. Friesen, L. Ibing, M. Winter, S. Nowak, *Electrochim. Acta* **2020**, *338*, 135894.
[50] A. Ghaur, F. Pfeiffer, D. Diddens, C. Peschel, I. Dienwiebel, L. Du, L. Profanter, M. Weiling, M. Winter, T. Placke, S. Nowak, M. Baghernejad, *Small* **2023**, *19*(44), 2302486.
[51] T. Dagger, M. Grützke, M. Reichert, J. Haetge, S. Nowak, M. Winter, F. M. Schappacher, *J. Power Sources* **2017**, *372*, 276–285.
[52] F. Horsthemke, A. Friesen, L. Ibing, S. Klein, M. Winter, S. Nowak, *Electrochim. Acta* **2019**, *295*, 401–409.
[53] G. N. Rimondino, J. A. Vila, F. E. Malanca, *J. Photochem. Photobiol., A* **2023**, *444*, 114994.
[54] G. N. Rimondino, W. J. Peláez, F. E. Malanca, *J. Phys. Chem. A* **2020**, *124*(1), 56–62.
[55] M. Bilde, T. E. Møgelberg, J. Sehested, O. J. Nielsen, T. J. Wallington, M. D. Hurley, S. M. Japar, M. Dill, V. L. Orkin, T. J. Buckley, R. E. Huie, M. J. Kurylo, *J. Phys. Chem. A* **1997**, *101*(19), 3514–3525.
[56] S. Parisotto, E. Azzi, A. Lanfranco, P. Renzi, A. Deagostino, *Reactions* **2022**, *3*(2), 233–253.
[57] B. D. W. Allen, M. D. Hareram, A. C. Seastram, T. McBride, T. Wirth, D. L. Browne, L. C. Morrill, *Org. Lett.* **2019**, *21*(22), 9241–9246.
[58] J.-J. Li, M.-M. Gao, G. Zhang, X.-H. Wang, S.-G. Wang, C. Song, Y.-Y. Xu, *Bioresour. Technol.* **2015**, *177*, 74–79.
[59] S. C. S. Wang, D. N. Bennion, *J. Electrochem. Soc.* **1983**, *130*(4), 741.
[60] D. Ouyang, K. Wang, Y. Pang, Z. Wang, *J. Power Sources* **2022**, *529*, 231247.
[61] J. Kalhoff, D. Bresser, M. Bolloli, F. Alloin, J.-Y. Sanchez, S. Passerini, *ChemSusChem* **2014**, *7*(10), 2939–2946.
[62] F. Pfeiffer, A. Griggio, M. Weiling, J.-F. Wang, F. Reißig, C. Peschel, L. Pillatsch, S. Warrington, S. Nowak, V. Grimaudo, I. Wright, M. Baghernejad, *Adv. Energy Mater.* **2024**, 2402187.
[63] F. Zapata, C. García-Ruiz, *Spectrochim. Acta, Part A* **2018**, *189*, 535–542.
[64] A. Kolesnikov, M. Kolek, J. F. Dohmann, F. Horsthemke, M. Börner, P. Bieker, M. Winter, M. C. Stan, *Adv. Energy Mater.* **2020**, *10*(15), 2000017.
[65] X. Zhang, P. N. Ross, R. Kostecki, F. Kong, S. Sloop, J. B. Kerr, K. Striebel, E. J. Cairns, F. McLarnon, *J. Electrochem. Soc.* **2001**, *148*(5), A463.
[66] E. M. Shembel, R. D. Apostolova, A. S. Strizhko, A. I. Belosokhov, A. F. Naumenko, V. V. Rozhkov, *J. Power Sources* **1995**, *54*(2), 421–424.

Batteries & Supercaps

Research Article
doi.org/10.1002/batt.202400568

Chemistry Europe
European Chemical
Societies Publishing

[67] E. Krämer, T. Schedlbauer, B. Hoffmann, L. Terborg, S. Nowak, H. J. Gores, S. Passerini, M. Winter, *J. Electrochem. Soc.* **2013**, *160*(2), A356–A360.

[68] P. Meister, X. Qi, R. Kloepsch, E. Krämer, B. Streipert, M. Winter, T. Placke, *ChemSusChem* **2017**, *10*(4), 804–814.

[69] D. Huang, C. Engtrakul, S. Nanayakkara, D. W. Mulder, S.-D. Han, M. Zhou, H. Luo, R. C. Tenent, *ACS Appl. Mater. Interfaces* **2021**, *13*(10), 11930–11939.

[70] F. Demelash, A. Arifiadi, B. Heidrich, E. Adhitama, C.-T. Lechtenfeld, N. M. Abke, M. Weiling, J. F. Wang, D. Diddens, S. Wiemers-Meyer, M. Winter, M. Baghernejad, P. Niehoff, *Energy Storage Mater.* **2024**, *72*, 103735.

[71] B. A. Sadeghi, C. Wölke, F. Pfeiffer, M. Baghernejad, M. Winter, I. Cekic-Laskovic, *J. Power Sources* **2023**, *557*, 232570.

[72] J.-P. Schmiegel, M. Leißing, F. Weddeling, F. Horsthemke, J. Reiter, Q. Fan, S. Nowak, M. Winter, T. Placke, *J. Electrochem. Soc.* **2020**, *167*(6), 060516–060516.

[73] S. Buechele, E. Logan, T. Boulanger, S. Azam, A. Eldesoky, W. Song, M. B. Johnson, M. Metzger, *J. Electrochem. Soc.* **2023**, *170*(1), 010518.

[74] T. Boetticher, A. Adamson, S. Buechele, E. D. Alter, M. Metzger, *J. Electrochem. Soc.* **2023**, *170*(6), 060507.

[75] T. Boulanger, A. Eldesoky, S. Buechele, T. Taskovic, S. Azam, C. Aiken, E. Logan, M. Metzger, *J. Electrochem. Soc.* **2022**, *169*(4), 040518.

[76] A. Adamson, K. Tuul, T. Bötticher, S. Azam, M. D. L. Garayt, M. Metzger, *Nat. Mater.* **2023**, *22*(11), 1380–1386.

[77] M. J. Frisch, G. W. Trucks, H. B. Schlegel, G. E. Scuseria, M. A. Robb, J. R. Cheeseman, G. Scalmani, V. Barone, G. A. Petersson, H. Nakatsuji, X. Li, M. Caricato, A. V. Marenich, J. Bloino, B. G. Janesko, R. Gomperts, B. Mennucci, H. P. Hratchian, J. V. Ortiz, A. F. Izmaylov, J. L. Sonnenberg, Williams, F. Ding, F. Lipparini, F. Egidi, J. Goings, B. Peng, A. Petrone, T. Henderson, D. Ranasinghe, V. G. Zakrzewski, J. Gao, N. Rega, G. Zheng, W. Liang, M. Hada, M. Ehara, K. Toyota, R. Fukuda, J. Hasegawa, M. Ishida, T. Nakajima, Y. Honda, O. Kitao, H. Nakai, T. Vreven, K. Throssell, J. A. Montgomery Jr., J. E. Peralta, F. Ogliaro, M. J. Bearpark, J. J. Heyd, E. N. Brothers, K. N. Kudin, V. N. Staroverov, T. A. Keith, R. Kobayashi, J. Normand, K. Raghavachari, A. P. Rendell, J. C. Burant, S. S. Iyengar, J. Tomasi, M. Cossi, J. M. Millam, M. Klene, C. Adamo, R. Cammi, J. W. Ochterski, R. L. Martin, K. Morokuma, O. Farkas, J. B. Foresman, D. J. Fox, *Gaussian 16 Rev. C.01*, Wallingford, CT **2016**.

[78] O. Borodin, M. Olguin, C. E. Spear, K. W. Leiter, J. Knap, *Nanotechnology* **2015**, *26*(35), 354003.

[79] A. V. Marenich, C. J. Cramer, D. G. Truhlar, *J. Phys. Chem. B* **2009**, *113*(18), 6378–6396.

[80] D. S. Hall, J. Self, J. R. Dahn, *J. Phys. Chem. C* **2015**, *119*(39), 22322–22330.

[81] M. Evertz, C. Lürenbaum, B. Vortmann, M. Winter, S. Nowak, *Spectrochim. Acta, Part B* **2015**, *112*, 34–39.